

Photocatalytic degradation of Direct Yellow 50 on TiO₂ and Fe³⁺-doped TiO₂ semiconductor nanoparticles under UV light irradiation

Mahmoud G.E.A.* and L. F. M. Ismail

Chemistry Department Faculty of Science, Al-Azhar University, Nasr City, Cairo, Egypt
mamygg@rocketmail.com

Abstract: Fe³⁺-doped TiO₂ composite nanoparticles (Fe³⁺ = 0.01wt %) were successfully synthesized using an incipient wet impregnation method in order to prevent penetration of the dopant cation into the bulk of TiO₂. The prepared nanoparticles were characterized by SEM, EDX, XRD and TEM. Results show that the size of Fe³⁺/TiO₂ particles decreases on doping with Fe³⁺ and their XRD peaks are broadened. Doping Fe³⁺ can control the conversion of TiO₂ from anatase to rutile. The photocatalytic degradation of Direct Yellow 50 was used as a model reaction to evaluate the photocatalytic activity of TiO₂ and Fe³⁺-doped TiO₂ nanoparticles. The doping amount of Fe³⁺ remarkably affects the activity of the catalyst. The degradation of dye depends on several parameters such as pH, catalyst, substrate and H₂O₂ concentrations. Electrical energy per order (EE/O) was proposed to assess the relative performance of catalytic system used. The adsorption of direct yellow 50, onto TiO₂ Degussa P25 from aqueous solution was investigated. The experimental data were analyzed by Langmuir and Freundlich models of adsorption. It was found that Langmuir equation fit better than Freundlich equation. The kinetics of the adsorption with respect to the initial dye concentration, were also investigated.

[Mahmoud G.E.A. and L. F. M. Ismail. **Photocatalytic degradation of Direct Yellow 50 on TiO₂ and Fe³⁺-doped TiO₂ semiconductor nanoparticles under UV light irradiation.** *J Am Sci* 2012;8(10):83-99]. (ISSN: 1545-1003). <http://www.jofamericanscience.org>. 14

Key words: DY50, Fe³⁺-doped TiO₂, photocatalysis, adsorption.

1. Introduction

It has shown a capacious prospect to generate clean environment using photocatalyst. Among the new oxidation methods called “advanced oxidation processes” (AOPs), heterogeneous photocatalysis using titanium dioxide (TiO₂) as a photocatalyst is highly considered a promising destructive technology for the treatment of polluted air and water because of a number of advantages [1-6]. Firstly, this process can destroy the polluting compounds by decomposing into ending non-toxic substances with the aid of light irradiation in UV or near-UV region. Secondly, environmentally friendly materials can be employed as a semiconductor photocatalyst, especially the most widely used TiO₂. Thirdly, this process can be carried out under mild conditions, i.e. room temperature and atmospheric pressure. Fourthly, it can bring about the complete degradation of most organic pollutants, without causing the secondary pollution problems. Finally, it is currently receiving an increasing attention because of the use of sunlight as the clean and renewable source of irradiation light with energy equal to or greater than the band gap energy of the TiO₂ photocatalyst (~3.2 eV for the anatase phase TiO₂). When the photocatalyst absorbs the irradiating light with suitable wavelengths, the electrons and holes are produced and transferred along the crystalline lattice to the photocatalyst surface. The electrons and holes trapped on the photocatalyst surface can react with both water and dissolved oxygen molecules to generate several oxygen active species, such as °OH, OH₂°, O₂°

–, and H₂O₂. These active species can further attack organic dye molecules to cause them decomposed. The detailed mechanisms for the photocatalytic dye degradation using the TiO₂ photocatalyst have already been demonstrated in a number of literatures [2, 4-12]. However, the large band gap ($E_g = 3.2$ eV) in TiO₂, activated only by ultraviolet (UV) light, low efficiency in utilizing solar energy and high recombination rate of the photo-generated electron/hole pairs result in the low efficiency in utilizing photon and hinder its further application in industry. In order to solve these problems, many methods have been applied to the modification of TiO₂, such as modification by noble metal [13, 14], semiconductor junctions [15], polymer-[16] and transition metal-doping [17]. Among these methods, transition metal doping has been studied extensively, and this technology has been applied to the degradation of dye, nitric oxide, polythene film and organic pollutants [13].

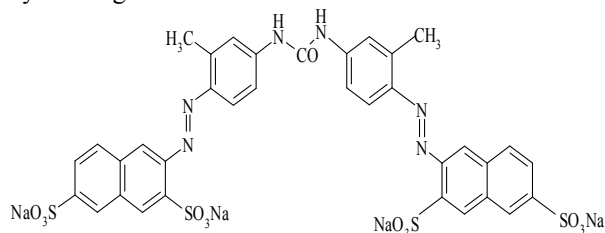
This work investigates the use of an AOP to break down the azo dye Direct Yellow 50. The action of TiO₂ Degussa P25 and Fe³⁺-doped TiO₂ (0.01% wt% Fe³⁺) nanoparticles under UV light irradiation at a wavelength of 254 nm will be compared in a laboratory-scale photoreactor. Direct Yellow 50 has been selected as a recalcitrant model pollutant because it is currently used in paper and textile industries and is present in their effluents. The morphological structure of the photocatalysts was examined by scanning electron microscope (SEM), energy dispersive X-ray spectroscopy (EDX), transmission electron microscopy

(TEM) and X-ray diffraction (XRD), and the degradation of dyes depends on several other parameters such as pH, concentrations of catalyst, substrate and H_2O_2 . Electrical energy per order (EE/O) was proposed to assess the relative performance of each catalytic system used. It was found that EE/O decreases with increasing the value of k_{app} . The adsorption of direct yellow 50 (DY50), onto TiO_2 Degussa P25 from aqueous solution was also investigated.

2. Experimental

2.1. Dye solutions:

C.I. Direct Yellow 50 (DY50) is diazo dye of the molecular weight 991.82 g/mol (Scheme 1). The dye is purchased from Ciba-Geigy. It is a water-soluble dye. The stock solution of DY50 is prepared by dissolving the accurately weighed amount of dye in 1 L of deionised water. All working solutions are prepared by diluting the stock solution with deionised water.



Scheme 1: C.I. Direct Yellow 50 (DY50)

2.2. Preparation of the Fe^{3+} -doped TiO_2 :

Doping was performed by an incipient wet impregnation method in order to prevent penetration of the dopant cations into the bulk of TiO_2 , since bulk doping increases the recombination rate of charge carriers resulting in a decrease in photocatalytic activity. 8g TiO_2 Degussa P25 and appropriate amount of $\text{Fe}(\text{NO}_3)_3 \cdot 9\text{H}_2\text{O}$ were mixed with definite volumes of doubly distilled water and stirred for 1h. During this

period, the mixture changed color into a light brownish beige depending upon the Fe^{3+} concentration. Three different Fe^{3+} -doped photocatalysts containing 0.01, 0.04 and 0.06 wt% Fe^{3+} were prepared. Then, the prepared photocatalysts were washed with water three times, heat-treated at 100°C for 24h to eliminate water, calcined at 500°C for 4h, ground and sieved [18]. The photocatalytic activity increases at doping amount of 0.01 wt% Fe^{3+} and then decreases with the further increase of the amount. So the characterization and photocatalytic activity of doping amount of 0.01 wt% Fe^{3+} are only investigated in this study.

2.3. Chemicals for pH adjustment

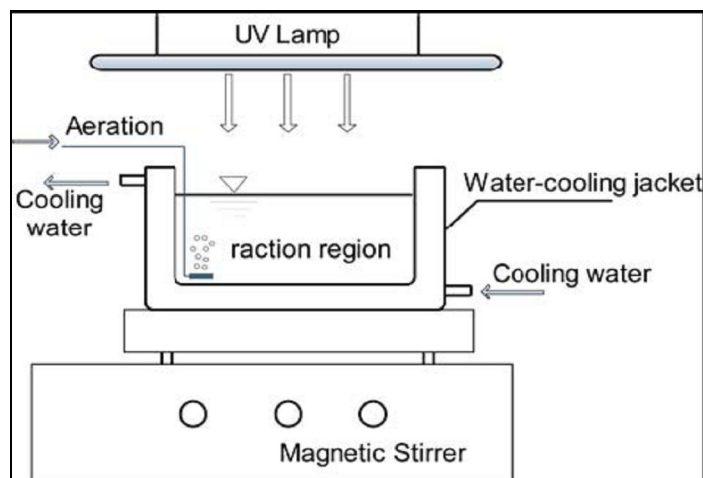
For the pH adjustment, concentrated reagent grade sulphuric acid and sodium hydroxide solutions (Panreac) were used. All solutions were prepared with deionised water obtained from a Millipore Milli-Q system.

2.4. The TiO_2 Degauss P25 (30 nm particle size, Germany) was used a photocatalyst.

Other chemicals; H_2O_2 and $\text{Fe}(\text{NO}_3)_3 \cdot 9\text{H}_2\text{O}$ from BDH or Merk are used as received.

2.5. Batch type photoreactor

All experiments were conducted in a 500ml thermostated batch glass reactor (Scheme 2) equipped with a magnetic stirrer. The light source was low pressure mercury lamp (2 lamps each of 4 watt) which basically emits at 254nm, used as artificial light source. The reaction mixture inside the cell, consisting of 250ml of dye sample and the precise amount of reagent, was continuously stirred with a magnetic bar and the temperature fixed at the required level (25°C). The intensity of the incident light, measured employing a uranyl actinometer [19], was $0.9675 \mu\text{Einstein} \times 10^{-5} \text{ s}^{-1}$. All experiments were carried out using 2 UV lamps each of 4watt at distance 20cm apart from the reaction mixture.



Scheme 2: Experimental setup for the photocatalytic dye degradation.

2.6. Equilibrium studies

2.6.1. Batch equilibrium experiments

Different DY50 concentrations are freshly prepared in deionized water. The experiments are carried out by shaking TiO₂, in a conical flask at 25°C in a thermostatted shaker bath in dark. The amount of dye in the solution was monitored by UV-Visible absorption spectroscopy until the absorbance values at λ_{\max} (397nm) remained constant. The initial and after time and equilibrium dye concentrations (C_o , C_t and C_e , respectively) are determined using a calibration curve based on absorbance at λ_{\max} 397nm versus dye concentration in standard DY50 solutions. (Eqs. 1 and 2) is used to calculate the amount of dye adsorbed at equilibrium (q_e) and at time t (q_t) (mg/g TiO₂) [20].

$$q_e = (C_o - C_e)(V/W) \quad (1)$$

$$q_t = (C_o - C_t)(V/W) \quad (2)$$

In (Eqs. 1 and 2) C_o , C_e and C_t are the initial, equilibrium and at time t solution concentrations (mg/l), respectively, and V is the volume of the dye solution (l) and W is the weight of TiO₂ (g) used.

2.7. Catalyst characterization:

2.7. 1. Experimental techniques:

The surface morphology of TiO₂ Degussa P25 and Fe³⁺-doped TiO₂ (0.01% wt% Fe³⁺) samples were examined using JEOL SEM – 25 scanning electron microscope. Prior to examination, the samples were dried under sputter coated gold.

The EDX pattern of TiO₂ Degussa P25 and Fe³⁺-doped TiO₂ (0.01% wt% Fe³⁺) were examined using OXFORD link ISIS Energy Dispersive X-ray Spectroscopy.

The TEM of TiO₂ Degussa P25 and Fe³⁺-doped TiO₂ (0.01% wt% Fe³⁺) measurements were examined with a JEM-100 CX (JEOL Ltd.).

The X-ray diffraction patterns of TiO₂ Degussa P25 and Fe³⁺-doped TiO₂ (0.01% wt% Fe³⁺) samples were measured with a modern Shimadzu Diffractometer x D-D1 Series. The X-ray copper target tube was operated at 40KV and 30mA and all the diffraction patterns were examined at room temperature and under constant operating conditions.

The absorption spectra were recorded with UV-9200 UV-VIS spectrophotometer. The absorbance of solutions measured at λ_{\max} (397 nm) using 1 cm quartz cell.

The pH values of the solutions were adjusted using Multimeter; WTW (Wissenschaftlich-Technische werkstätten GmbH) InoLab Multi Lev11, ba 12237de; Germany.

3. Results and discussion

3. 1. Morphological and compositional analyses of TiO₂ Degussa P25 and Fe³⁺-doped TiO₂:

3.1.1. SEM morphologies of TiO₂ Degussa P25 and Fe³⁺-doped TiO₂:

Figure 1 shows the SEM micrographs obtained for the TiO₂ Degussa P25 and Fe³⁺-doped TiO₂ (0.01% wt% Fe³⁺). Figure 1a shows that TiO₂ Degussa P25 consists of homogeneous, regular and polyhedral particles. In contrast, the Fe³⁺-doped TiO₂ consists of smaller particles, with straight edges and sharp corners.

3.1. 2. EDX spectra of TiO₂ Degussa P25 and Fe³⁺-doped TiO₂:

Figure 2 shows the EDX spectra of TiO₂ Degussa P25 and Fe³⁺-doped TiO₂ (0.01% wt% Fe³⁺). The obtained amount in EDX analysis is in agreement with the doping contents. The EDX results also indicate an almost uniform distribution of Fe³⁺ cations between the particles.

3.1. 3. TEM of TiO₂ Degussa P25 and Fe³⁺-doped TiO₂:

Figure 3 shows the TEM of TiO₂ Degussa P25 and Fe³⁺-doped TiO₂ (0.01% wt% Fe³⁺). From Figures 3, the average particle sizes are 40.3 and 33.7 for TiO₂ Degussa P25 and Fe³⁺-doped TiO₂ (0.01% wt% Fe³⁺), respectively. The sizes obviously decrease with doping of Fe³⁺. These results reveal that the Fe³⁺ doping restrains the growth of the TiO₂ crystal grains, resulting in a decrease in particle size [21] and an increase in the surface energy, which may cause agglomeration between the crystal grains.

3.1. 4. XRD analysis of TiO₂ Degussa P25 and Fe³⁺-doped TiO₂:

Figure 4 shows the XRD patterns of TiO₂ Degussa P25 and Fe³⁺-doped TiO₂ (0.01% wt% Fe³⁺). The XRD diffractogram of the TiO₂ P25 (Figure 4a) shows the presence of both anatase and rutile phases. The molar fractions of both phases are 79% anatase and 21% rutile. As shown in Figure 4a, the peaks at 2θ 25.31, 37.81 and 48.01 elucidate the diffractions of the (101), (004) and (200) anatase-type TiO₂ with the main XRD diffractogram at 25.31. Characteristic peak of rutile TiO₂ is found at 2θ 27.51 [22]. It can be seen from Figure 4 that (1) The presence of iron catalyzes the anatase to rutile transformation, with rutile being detected [13]. These results reveal that the doping Fe³⁺ controls the crystalline conversion of TiO₂ from rutile to anatase phase. The diffraction peaks are remarkably broadened. There are some factors affecting the broadening of diffraction peaks, such as the grain size, the defect of the crystal. From the results of the sample's TEM, it can be concluded that the small grain size is one of the factors resulting from the broadening of diffraction peaks. The characteristic peaks of Fe₂O₃ are not observed in the studied range of doping amount of Fe³⁺. One of the reasons may be the homogeneous dispersion of Fe³⁺ in the TiO₂ lattice because of the similar ion radii of

Fe^{3+} and Ti^{4+} , and the other is that the amount of doped Fe^{3+} is so low that it can not be detected by XRD or the weak diffraction peaks of Fe_2O_3 are shielded by the broadened diffraction peaks of TiO_2 .

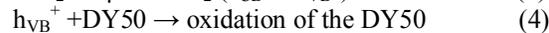
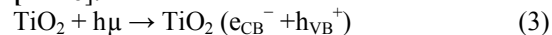
3. 2. Parameters affecting the photocatalytic degradation of DY50 using TiO_2 -P25 :

3. 2.1. Effect of catalyst loading:

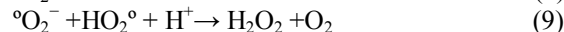
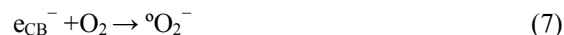
Photocatalytic process of DY50 with different catalyst loading was investigated after being submitted to adsorption onto TiO_2 -P25 surfaces. The dark experiment results in a decrease on the absorbance at λ_{max} 397nm of more than 33%, after 30min suggesting the adsorption of the DY50 onto TiO_2 surfaces. Experiments are carried out with different concentrations of catalyst (0.25, 0.50 1.00 and 1.50 g/l) at fixed DY50 concentration (0.02mM) and pH 3.0. These experimental conditions are chosen to analyze the possibility of the simultaneous DY50 photodegradation when adsorbed onto the TiO_2 -P25 surface and in solution. The color removal efficiency (Figures 5a) for DY50 increases from 80.56 % to 92.78 at 65 min of irradiation time when the catalyst concentration is increased from 0.25 to 1.0 g/l and then it decreases. These results show that TiO_2 -P25 is reasonably effective in photodegrading DY50, as denoted by the decrease of the band intensity. It is clear from the investigations that catalyst loading is an important factor that can significantly influence the photocatalytic degradation of DY50. The experimental kinetic data follow the pseudo first order kinetic, which is rationalized in terms of the Langmuire-Hinshelwood model modified to accommodate reactions occurring at a solid-liquid interface [23]. Plot of $\ln A/A_0 = -k_{\text{ap}} t$ is given in Figure 5b. In general a good correlation is obtained, suggesting that the reaction kinetics follows a pseudo-first order rate law. The slopes of the straight lines passing through the origin yield the apparent rate constants (k_{ap}) depicted in Table 1. This Table also gives the maximum degradation %.

Hence, the results obtained for the presented catalyst loading reveal that, the reaction rate constant increases with increasing catalyst's loading up to a level 1.0 g/l which corresponds to the optimum of light absorption. These results demonstrated that both UV light and a photocatalyst, such as TiO_2 are needed for the effective destruction of DY50, because it has been established that the photocatalytic degradation of organic matter in solution is initiated by photoexcitation of the semiconductor, followed by the formation of an electron-hole pair on the surface of catalyst (Eq. (3)). The high oxidative potential of the hole (h_{VB}^+) in the catalyst permits the direct oxidation of organic matter (DY50) to reactive intermediates (Eq. (4)). Very reactive hydroxyl radicals can also be formed either by the decomposition of water (Eq. (5))

or by the reaction of the hole with OH^- (Eq. (6)). The hydroxyl radical is an extremely strong, non-selective oxidant that leads to degradation of organic chemicals [24-26]:



Moreover, electron in the conduction band (e_{CB}^-) on the catalyst surface can reduce molecular oxygen to superoxide anion (Eq. (7)). This radical, in the presence of organic scavengers, may form organic peroxides (Eq. (8)) or hydrogen peroxide (Eq. (9)):



Electrons in the conduction band are also responsible for the production of hydroxyl radicals, which have been indicated as the primary cause of organic matter mineralization (Eq. (10)) [2, 27]:



3. 2.2. Effect of DY50 concentration

Successful application of photocatalytic oxidation system requires the investigation of the dependence of photocatalytic degradation rate on the substrate concentration (C_o) [28, 29].

The effect of initial DY50 concentrations is examined in concentration rang of 0.02 to 0.50mM after being submitted to adsorption onto TiO_2 on the photocatalytic degradation of DY50 under UV light irradiation. The dark experiment results in a decrease on the degradation degree calculated at λ_{max} 397nm after 30min suggesting the adsorption of the dye at TiO_2 surfaces. The photocatalytic efficiency of 1.0g/l of TiO_2 nanomaterial on the decolorization of DY50 solution is examined at pH 3.0 to analyze the possibility of the simultaneous DY50 photodegradation. With the increase in the substrate concentration, the degradation efficiency decreased from 92.64% to 4.41%.

Moreover, the initial rate of photodegradation is high at the lower concentration range but it decreases as concentration increases. Generally the photocatalytic reaction follows a Langmuir-Hinshelwood mechanism [23]. The linear transforms $\ln A / A_0 = -k_a t$ are given in Figure 6. In general a good correlation is obtained, suggesting that the reaction kinetics follows a pseudo-first order rate law. The slopes of the straight lines passing through the origin yield the apparent rate constants (k_{ap}) depicted in Table 2. It has been indicated in several

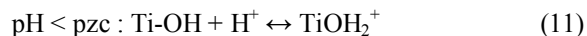
investigations that as the concentration of the target pollutant increases, more and more molecules of the compound are adsorbed on the surface of the photocatalyst [27]. Therefore, the reactive species ($^{\circ}\text{OH}$ and $^{\circ}\text{O}_2^-$) required for the degradation of the pollutant also increases. However, the formation of $^{\circ}\text{OH}$ and $^{\circ}\text{O}_2^-$ on the catalyst surface remains constant for a given light intensity, catalyst amount and duration of irradiation. Hence, the available OH radicals are inadequate for pollutant degradation at higher concentrations. In addition, an increase in substrate concentration can lead to the generation of intermediates, which may adsorb on the surface of the catalyst. Slow diffusion of the generated intermediates from the catalyst surface can result in the deactivation of active sites on the photocatalyst and result in a reduction in the degradation rate. This is in accordance with the Langmuire Hinshelwood (L-H) law [23]. Several investigations have described the dependence of the photocatalytic degradation rates on the concentration of various phenols and dyes using the L-H kinetics model [28-30].

3. 2. 3. Effect of the pH value

The photocatalytic degradation of DY50 are conducted at different pH values (pH = 1.1-9.3) and dye concentration 0.02 mM at catalyst loading of 1.0 g/l. The degradation degrees of the dye in the different pH media are given in Figure 7a. Increase of the dye solution pH from 1.1 to 3.0 increases the degradation from 74.69% to 92.64% within 65 min of irradiation time and then it decreases to 36.23% when the pH increases to 7.0. In alkaline medium (pH = 9) the degradation degree increases to 50.21%

The interpretation of pH effects on the efficiency of dye photodegradation process is a very difficult task because of its multiple roles [6]. First, is related to the ionization state of the surface. The point of zero charge (pzc) for titanium dioxide is at pH 6.5.

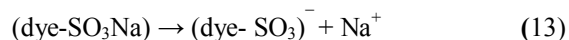
In acidic solution the pH is lower than pzc and hence the TiO_2 surface is positively charged.



In basic solution the surface is negatively charged as given in following equation:



On the other hand, the dye contain sulphonate group, so that hydrolyzed molecule behaves as anionic dye.



pH changes can thus influence the adsorption of dye molecules onto the TiO_2 surfaces, an important step for the photocatalytic oxidation to

take place. **Bahnmann et al.** [31] have already reviewed that acid-base properties of the metal oxide surfaces can have considerable implications upon their photocatalytic activity. Second, hydroxyl radicals can be formed by the reaction between hydroxide ions and positive holes. The positive holes are considered as the major oxidation species at low pH, whereas hydroxyl radicals are considered as the predominant species at neutral or high pH levels [32]. It was stated that in alkaline solution, $^{\circ}\text{OH}$ are easier to be generated by oxidizing more hydroxide ions available on TiO_2 surface, thus the efficiency of the process is logically enhanced [33]. Similar results are reported in the photocatalyzed degradation of acidic azo dyes and triazine containing azo dyes [34– 36].

Moreover, the mechanism of the photocatalytic reaction in the presence of TiO_2 consists of a free radical reaction initiated by UV light [37]. The mechanism may depend on the ability of the degraded compound to be adsorbed on the surface of the catalyst. The extent of such adsorption depends on many factors, and one of it is the charge of the degraded compound. It was found that in photocatalytic degradation, the adsorption level on unmodified TiO_2 is higher for dyes with a positive charge (cationic) than for those with a negative charge (anionic) [38]. As the charge depends on the pH of a given solution, it follows that both pH and the nature of a particular dye influence the photocatalyst activity [36, 39-41].

The degradation rate of DY50 increases with decrease in pH (pH= 3.0)[2]. At pH <6, a strong adsorption of the anionic dye on the TiO_2 particles is observed as a result of the electrostatic attraction of the positively charged TiO_2 with the anionic dye. At pH >6.8 as dye molecules are negatively charged in alkaline media, their adsorption is also expected to be affected by an increase in the density of TiO^- groups on the semiconductor surface. Thus, due to Coulombic repulsion, the dyes are scarcely adsorbed [5, 41] and the degradation decreases. It has earlier been reported that in alkaline medium, there is a greater probability for the formation of hydroxyl radical ($^{\circ}\text{OH}$), which can act as an oxidant, thus increasing the photodegradation of the dye [42].

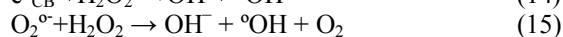
The photocatalytic oxidation kinetics of DY50 has often been modelled with the Langmuir–Hinshelwood equation, which also covers the adsorption properties of the substrate on the photocatalyst surface. [23].

The semi-logarithmic graphs of the pH versus irradiation time yield straight lines indicating pseudo-first order reaction (Figure 7b). The apparent reaction rate constants (k_{ap}) for photocatalytic degradation of DY50 are evaluated from experimental data using a linear regression. In all

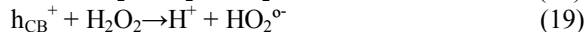
cases, r (correlation coefficient) values are higher than 0.99, which confirm the proposed kinetics for decolorization of dye in this process. The calculated apparent reaction rate constants (k_{ap}) are listed in Table 3.

3. 2. 4. Effect of H₂O₂

The photocatalytic degradation of DY50 has been studied at different hydrogen peroxide concentrations. The effect of varying the initial H₂O₂ dose from 5- 50 mM for DY50 concentration 0.02 mM at pH 3.0 on the degree of photodegradation is displayed in Figure 8. Generally the photocatalytic reaction follows a Langmuir–Hinshelwood mechanism. The linear transforms $\ln A_0/A = -k_{ap} t$ are given in Figure 8b. In general a good correlation is obtained, suggesting that the reaction kinetics follows a pseudo-first order rate law. The slopes of the straight lines passing through the origin yield the apparent rate constants (k_{ap}) depicted in Table 4. The degradation rate of DY50 increases with increasing H₂O₂ concentration up to 10 mM, above this value the degradation rate decreases. H₂O₂ increases the rate of hydroxyl radical formation through three ways: Firstly, it could act as an alternative electron acceptor to oxygen [43] (Eq. (14)), which might restrain the bulk composite of the photo-excited electrons and holes. This should consequently increase the rate of the photocatalytic process. Secondly, the reduction of H₂O₂ at the conductance band would also produce hydroxyl radicals. Even if H₂O₂ was not reduced at the conductance band it can accept an electron from superoxide again producing hydroxyl radicals (Eq. (15)). Thirdly, the self-decomposition by illumination will also produce hydroxyl radicals (Eq. (16) [44]:



At high concentration, the hydrogen peroxide adsorbed on the photocatalytic surface can effectively scavenge not only the photocatalytic surface formed ${}^{\circ}OH$ radicals (Eqs. (17) and (18) but also the photo-generated holes (h_{CB}^+) (Eq. (19)) and thus inhibit the major pathway for heterogeneous generation of ${}^{\circ}OH$ radicals:



It is worth mentioning here that HO_2° radicals are less reactive than ${}^{\circ}OH$, therefore, have negligible contribution in the dye degradation. Therefore, the proper addition of hydrogen peroxide could accelerate the photodegradation rate of DY50. However, in order to keep the efficiency of the added hydrogen peroxide, it is necessary to choose the

proper dosage of hydrogen peroxide, according to the kinds and the concentrations of the pollutants.

3. 2.5. Efficiency of Photodegradation

The evaluation of the efficiency of photodegradation treatment processes is difficult because the reaction rate depends on many factors. Thus, there is need for a figure of merit that can be used to assess the relative performance of each system. As a figure of merit, the electrical energy per order (EE/O) has been proposed, defined as the electrical energy (in kilowatt hours) required to reduce the concentration of a pollutant by one order of magnitude in 1000 US gallons (3785 L) of water. The EE/O value may be calculated from the following equation [44- 46]:

$$EE/O = (P \times (t/60) \times 3782) / (V \times \log(C_0/C_t)) \quad (20)$$

where P is the lamp power (in kilowatts), t is the irradiation time (in minutes), V is the reactor volume (in litres) and C_0 and C_t are the initial and final concentrations over the irradiation time. The EE/O values are related to the first-order rate constant, k_{ap} (per minute) by:

$$EE/O = 145.25 P / (V \times k_{ap}) \quad (21)$$

Data in tables 1-4 show that the value of EE/O (kWh) decreases with increasing the value of the k_{ap} . Low values of EE/O are obtained at the best condition for degradation ($[TiO_2] = 1.0$ g/l, 10.0 mM H₂O₂, pH = 3.0 and $[DY50] = 0.02$ mM). This indicates that using optimum condition in degradation of dyes relatively use low operational electric energy.

3.3. photocatalytic degradation of DY50 using Fe³⁺doped-TiO₂-P25:

The efficiency of Fe³⁺doped-TiO₂-P25 (Fe³⁺ wt%0.01) has been tested on the photodegradation of DY50 at $[DY50] = 0.02$ mM and pH 3.0 in presence of 1.0 g/l Fe³⁺doped-TiO₂-P25. These experimental conditions are chosen to analyze the possibility of the simultaneous DY50 photodegradation when adsorbed onto the Fe³⁺doped-TiO₂-P25 surfaces. After 65 min of photodecolorization, 99.503 % of the yellow color of the DY50 solution disappeared. Figure 9 shows degradation degree of DY50 upon irradiation in the presence of TiO₂-P25 and Fe³⁺doped-TiO₂-P25. Generally the photocatalytic reaction follows a Langmuir–Hinshelwood mechanism. The value the calculated rate constant of DY50 photodegradation in presence of Fe³⁺doped-TiO₂-P25 (Fe³⁺ wt%0.01) is $75.2 \times 10^{-3} \text{ min}^{-1}$. Compared with the pure TiO₂-P25 photocatalyst ($60.96 \times 10^{-3} \text{ min}^{-1}$), enhanced photocatalytic properties of the Fe³⁺doped-TiO₂-P25 nanoparticles can be observed as expected [47].

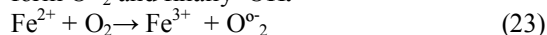
Data in Figure 9 shows that practically the 0.01wt% Fe³⁺-doped TiO₂ sample expressed higher initial activities than that of pure TiO₂ P25. This fact can be explained by the presence of Fe³⁺ making the

amount of active sites higher due to the formation of Fe-O-Ti bond in the TiO₂ crystal lattice, as well as the consequent formation of defects on the crystal surface that plays the role of a trap for preventing electron-hole recombination [13].

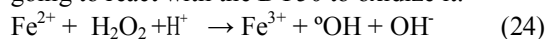
Moreover, metal ion doping influence the photo activity of TiO₂ by electron or hole traps. When trap can cause the formation of some active species that benefit degradation of dye, dopant introduction is positive effect. If dopant introduction cannot decrease e_{CB}^- and h_{VB}^+ recombination rate, the introduction is ineffective for the degradation. Fe³⁺ ions have an intense absorption in the UV-visible light region and make a red shift in the band gap transition of the Fe³⁺-doped TiO₂ resulting in production of more photo-generated electrons and holes to participate in the photocatalytic reactions. However, since e_{CB}^- and h_{VB}^+ recombination can occur quickly above 0.01wt% Fe³⁺ (preliminary experiment not presented), therefore, the degradation efficiency is low. At an appropriate doping concentration, Fe³⁺ ions may act a mediator of the transfer of interfacial charge. The experimental results show that the presence of a small amount of Fe³⁺ ions (0.01 wt %) can improve the photodegradation efficiency. This may be due to the following reasons. The electron scavenger effect of Fe³⁺, which prevents the recombination of e_{CB}^- and h_{VB}^+ results in increase of the efficiency of photodegradation process [13]. The possible reaction can be represented as:



Choi et al. [17] considered that the transition from Fe³⁺ to Fe²⁺ corresponds to the transition from d⁵ to d⁶, and Fe²⁺ is relatively unstable due to the loss of exchange energy and tends to return to Fe³⁺, resulting in the release of the trapped electron becoming easy. However, the Fe²⁺/Fe³⁺ energy level lies close to Ti³⁺/Ti⁴⁺ level. Because of this proximity, the trapped electron in Fe²⁺ can be easily transferred to a neighbouring surficial Ti⁴⁺ and combines with oxygen molecule to initiate the following reaction to form O[•]₂ and finally [•]OH.



Moreover, in the photocatalytic system, H₂O₂ may also be produced on TiO₂ surface as well [13]. The coexistence of Fe²⁺ and H₂O₂ in acidic media (Fenton's reaction) may produce [•]OH that acts as a strong oxidizing agent. After that, the [•]OH is going to react with the DY50 to oxidize it.



3.4. Adsorption Study of DY50 onto TiO₂-P25 surface

Since the photocatalytic degradation of dye occurs predominantly on the surface of photocatalyst

[48], studies on the adsorption of the DY50 from aqueous solution onto TiO₂-P25 nanoparticles are relevant and important. The equilibrium concentration of the dye (C_e) in contact with the catalyst, instead of that of the feed dye solution, represents the true dye concentration in solution at the start of irradiation. For this reason adsorption of the nanoparticles TiO₂-P25 in the dark is tested. It is observed that most of the adsorption for the nanoparticles occurs within 30 min.

3.4.1. The effect of contact time and initial dye concentration on the adsorption of DY50 onto TiO₂

The adsorption of different initial dye concentrations onto TiO₂ is investigated as a function of contact time in order to determine the equilibrium time for maximum adsorption. A plot of the amount of dye adsorbed per gram TiO₂ (q_t) (mg/g TiO₂) at any time versus contact time (t) is shown in Figure 10. It is found that the adsorption capacity is concentration dependent and increases with initial concentration of the DY50. An increase in the initial dye concentration lead to an increase in the amount of dye adsorbed onto TiO₂. This may be a result of an increase in the driving force of the concentration gradient with the increase in the initial dye concentration [49]. This indicate that the initial dye concentration plays an important role in the adsorption capacity of D onto TiO₂.

The equilibrium time is the time taken for the maximum adsorption of dye onto the TiO₂ surface, above which the adsorption remains constant. The equilibrium time was found to be about 30 min at pH 3.0. The adsorption is very fast at the initial stages of contact time until it remained constant.

3.4.2. Adsorption Isotherm

The correlation of equilibrium adsorption data by either theoretical or empirical equations is important in the design and operation of adsorption systems. Adsorption isotherms demonstrate the relationships between equilibrium concentrations of adsorbate in the solid phase q, and in the liquid phase C at constant temperature [50,51].

Adsorption isotherms are described in many mathematical forms. They are often obtained in the laboratory using batch tests in which the equilibrium data are attempted by various isotherm models such as Langmuir and Freundlich isotherms [52,53].

3.4.2.1. The Langmuir isotherm

The Langmuir isotherm has been widely used to describe single-solute systems. This isotherm assumes that intermolecular forces decrease rapidly with distance and consequently it can predict monolayer coverage of the adsorbate on the outer surface of the adsorbent. Further assumption is that adsorption occurs at specific homogeneous sites

within the adsorbent and there is no significant interaction among adsorbed species. The Langmuir isotherm is given by the following equation [54]:

$$q_e = QbC_e / (1 + bC_e) \quad (25)$$

a linear form of this expression is:

$$1/q_e = (1/Q) + (1/QbC_e) \quad (26)$$

where q_e is the amount of dye adsorbed per gram of TiO₂ (mg/g); C_e denotes the equilibrium concentration of dye in solution (mg/l), b represents the Langmuir constant (l/mg) that relates to the affinity of binding sites and Q is the theoretical saturation capacity of the monolayer (mg/g). The values of Q and b are calculated from the intercept and slope of the linear plot of $1/q_e$ versus $1/C_e$ (Figures 11). The Langmuir isotherm constants along with correction coefficients are reported in Table 5.

3.4.2.2. The Freundlich isotherm

Moreover, the Freundlich model is an empirical equation that assumes heterogeneous adsorption due to the diversity of adsorption sites. The Freundlich equation is [54]:

$$q_e = Q_f C_e^{1/n} \quad (27)$$

Eq. 6 can be linearized as:

$$\ln q_e = \ln Q_f + 1/n(\ln C_e) \quad (28)$$

where q_e is the equilibrium dye concentration (mg/g); C_e the equilibrium dye concentration in solution (mg/l); Q_f and n are the Freundlich constants, which represent the adsorption capacity and the adsorption strength, respectively. Q_f and $1/n$ can be obtained from the intercept and slope of the linear plot of $\ln(q_e)$ versus $\ln(C_e)$. From Figure 12 and Table 5 the magnitude of $1/n$ quantifies the favorability of adsorption and the degree of heterogeneity of TiO₂ surface. If $1/n$ is less than unity, indicating favorable adsorption, then the adsorption capacity increases and new adsorption sites occur.

3.4.3. Kinetics of adsorption

3.4.3.1. First order kinetic model

In order to examine the controlling mechanism of the adsorption process, pseudo first-order and pseudo second-order equations are used to test the experimental data.

The kinetic adsorption data are processed to understand the dynamics of the adsorption process in terms of the order of the rate constant. Kinetic data are treated with the pseudo-first order kinetic model of Lagergren based on solid capacity [55,56]. The Lagergren first-order model [55] is given by the following differential equation:

$$dq_t = k_1(q_e - q_t) \quad (29)$$

where q_e and q_t refer to the amount of dye adsorbed (mg/g) at equilibrium and at time t (min), respectively, and k_1 (min⁻¹) is the equilibrium rate constant of the pseudo-first order reaction. Integrating Eq. (28) for the boundary conditions $t=0$ to $t=t$ and $q_t=0$ to q_t , gives Eq. (29) which is the integrated rate law of pseudo-first order reaction.

$$\ln(q_{e1} - q_t) = \ln q_{e1} - k_1 t \quad (30)$$

Values of the rate constant k_1 and the equilibrium adsorption capacity q_{e1} could be respectively obtained from the slope and the intercept of the straight line representing the adsorption data. Figure 13 shows representative plots of $\ln(q_e - q_t)$ versus t at different dye concentrations and pH 3.0 in aqueous solution. Although the correlation coefficients, r_1 , for the application of the pseudo first-order model are reasonably high in some cases, all of the intercepts of the straight line plots do not yield predicted q_{e1} values equal, or even values reasonably close to experimental q_e values (Table 6).

3.4.3.2. Second order kinetic model

Kinetic data are further treated with pseudo second-order kinetic model [57, 58]. The differential equation is:

$$dq_t / (q_{e2} - q_t)^2 = k_2 dt \quad (31)$$

Where k_2 is the equilibrium rate constant of the pseudo-second order adsorption (g/mg min). Integration of Eq. (30) for the boundary conditions $t=0$ to $t=t$ and $q=0$ to q_e gives

$$t / (q_e - q_t) = 1/k_2 q_e^2 + t/q_e \quad (32)$$

where k_2 is the equilibrium rate constant of pseudo second-order adsorption (mg⁻¹ min⁻¹). If pseudo second-order kinetics is applicable, the plot of t/q_t versus t should show a linear relationship. The plot of the linearised form of the second-order model at different dye concentrations and pH 3.0 are given in Figure 14. The straight lines in the plot of t/q_t versus t show good agreement of experimental data with the second-order kinetic model for the DY50 (Table 6). The slopes and intercepts of plots are used to calculate the k_2 and q_{e2} . The correlation coefficients (r_2) for the second order rate kinetic model are higher than 0.99. The second-order rate constant, k_2 , and equilibrium adsorption capacity, q_{e2} , are calculated from the intercept and slope of the plots of t/q_t versus t . The calculated q_{e2} values agree very well with the experimental data (Table 6). These indicate that the adsorption of DY50 obeys pseudo second-order kinetic model. Hence, this study suggested that the pseudo-second-order kinetic model better represented the adsorption kinetics of DY50 onto cotton fiber.

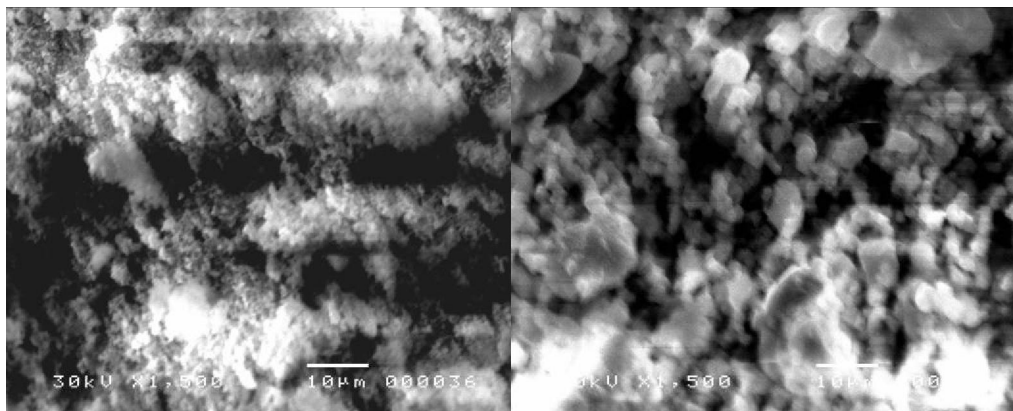


Figure 1: SEM micrographs for (a) TiO₂ Degussa P25 and (b) 0.01% wt% Fe³⁺-doped TiO₂.

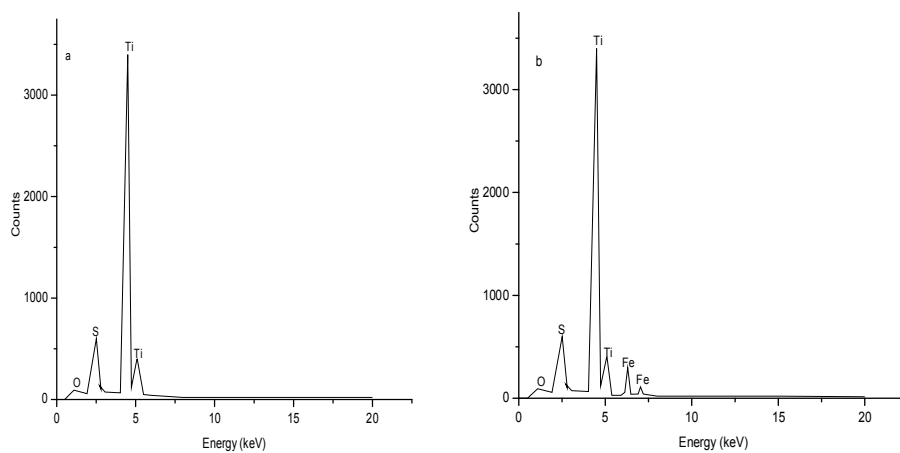


Figure 2: EDX spectra of the (a) TiO₂ Degussa P25 and (b) 0.01% wt% Fe³⁺-doped TiO₂.

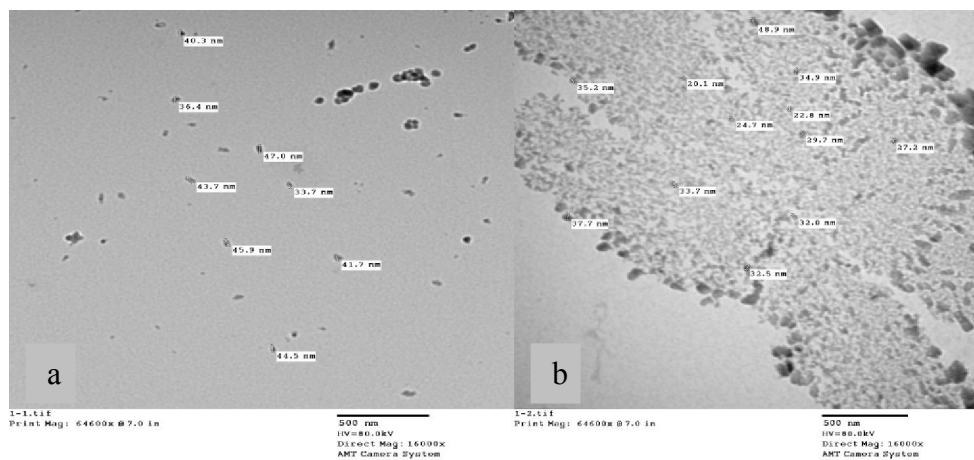


Figure 3: TEM images of (a) TiO₂ Degussa P25 and (b) 0.01% wt% Fe³⁺-doped TiO₂

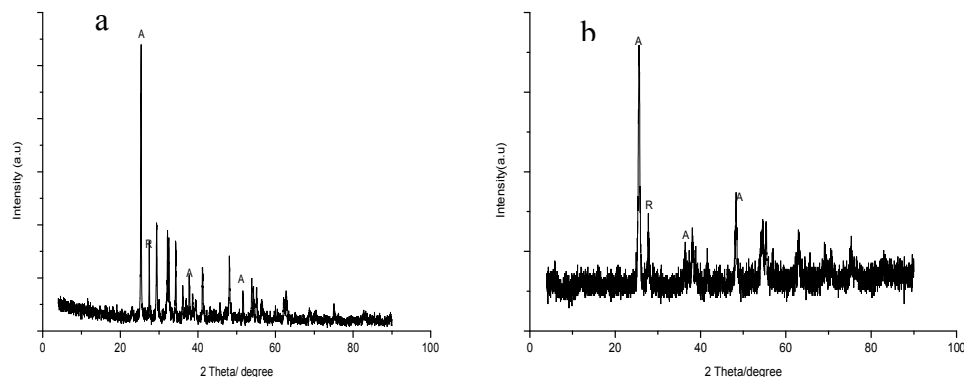


Figure 4: XRD diffractograms of the (a) TiO_2 Degussa P25 and (b) 0.01% wt% Fe^{3+} -doped TiO_2 (A: anatase and R: rutile).

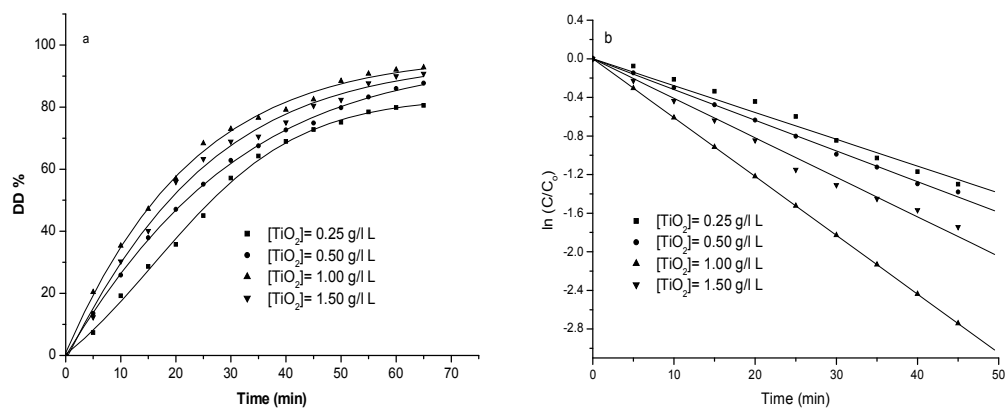


Figure 5: The effect of initial catalyst loading on the degree of degradation (DD%, a) and rate of dye degradation (b) in presence of $[\text{DY50}] = 0.02 \text{ mM}$ and $\text{pH } 3.0$.

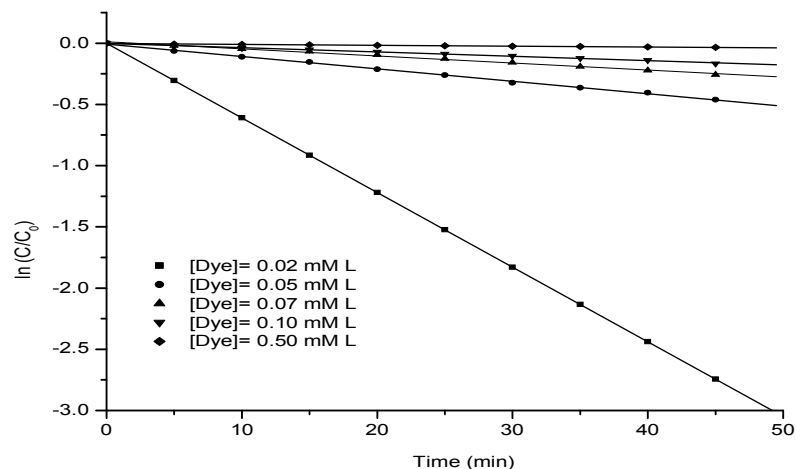


Figure 6: The effect of initial concentration of the dye on rate of dye degradation in presence of 1.0 g/l TiO_2 and $\text{pH } 3.0$.

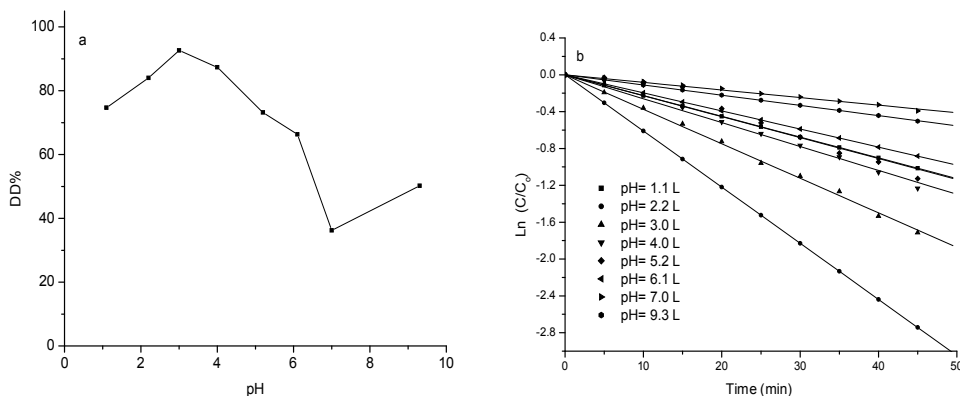


Figure 7: Effect of pH on (a) the degree of degradation of DY50 and (b) rate of dye degradation. Dosage of TiO_2 : 1.0 g/l, irradiation time: 65 min and dye concentration 0.02 mM.

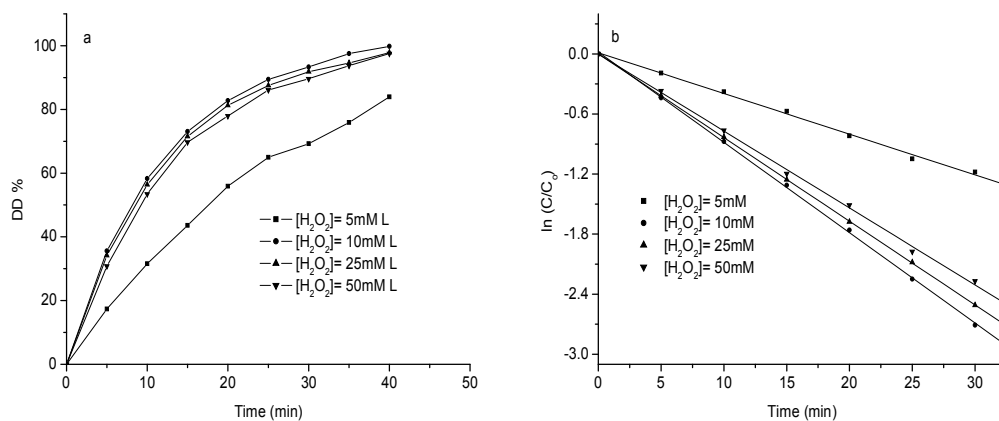


Figure 8: Effect of H_2O_2 concentrations on (a) the degree of degradation of DY50 and (b) rate of dye degradation. Dosage of TiO_2 : 1.0 g/l, irradiation time: 65 min and dye concentration 0.02 mM.

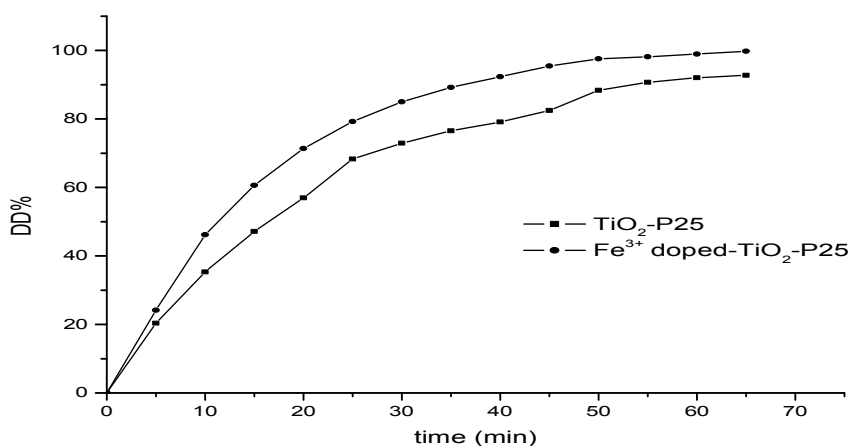


Figure 9: Effect of TiO_2 Degussa P25 and 0.01% wt% Fe^{3+} -doped TiO_2 (1.0 g/l) on the degree of degradation of DY50. Irradiation time: 65 min, dye concentration 0.02 mM and pH 3.

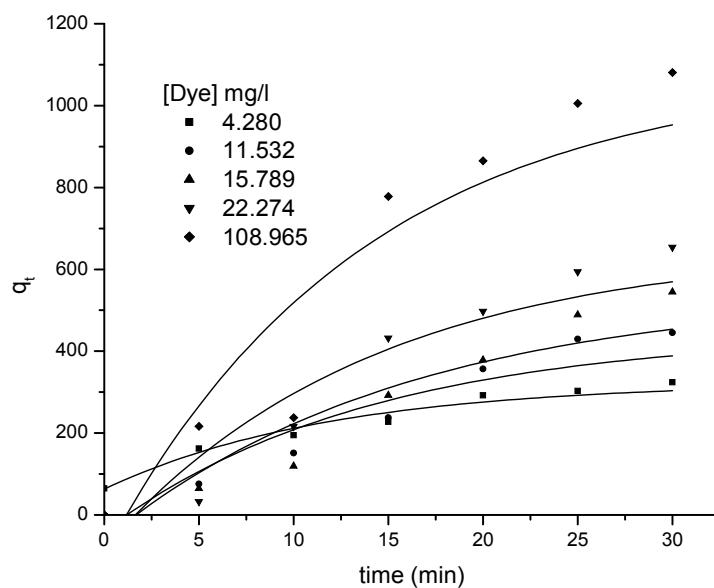


Figure 10: Effect of contact time on the adsorption of DY50 onto TiO₂ P25 at different dye concentrations at pH 3.0.

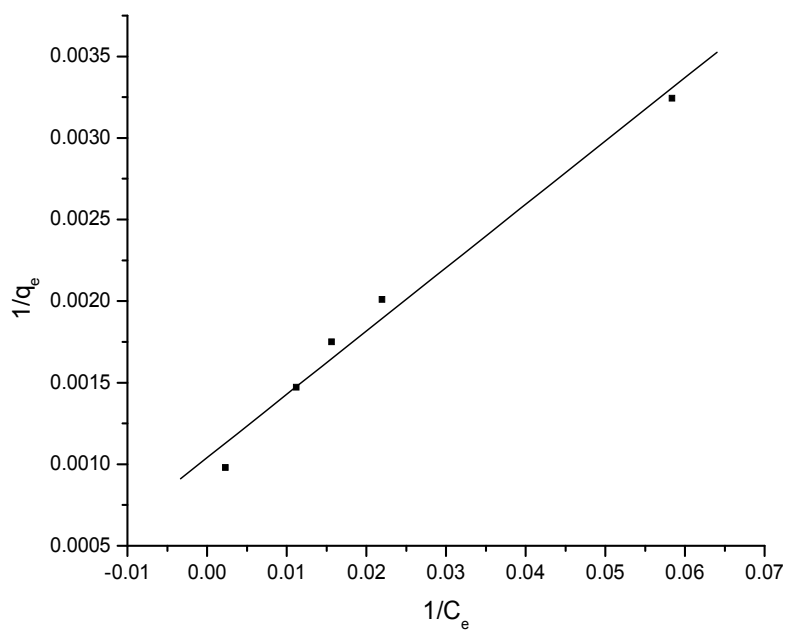


Figure 11: Langmuir adsorption isotherm plot for the adsorption of DY50 onto TiO₂-P25.

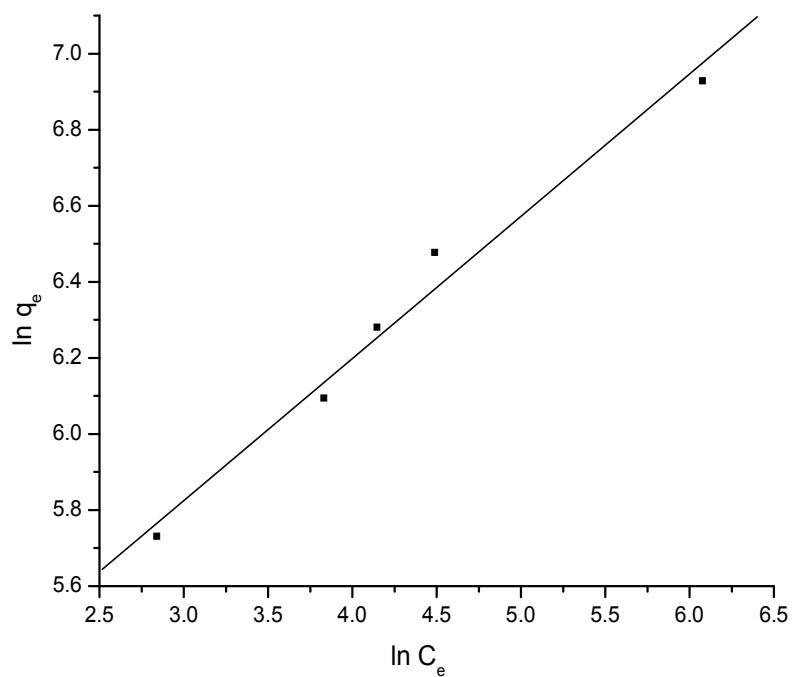


Figure 12: Freundlich adsorption isotherm plot for the adsorption of DY50 onto TiO_2 -P25.

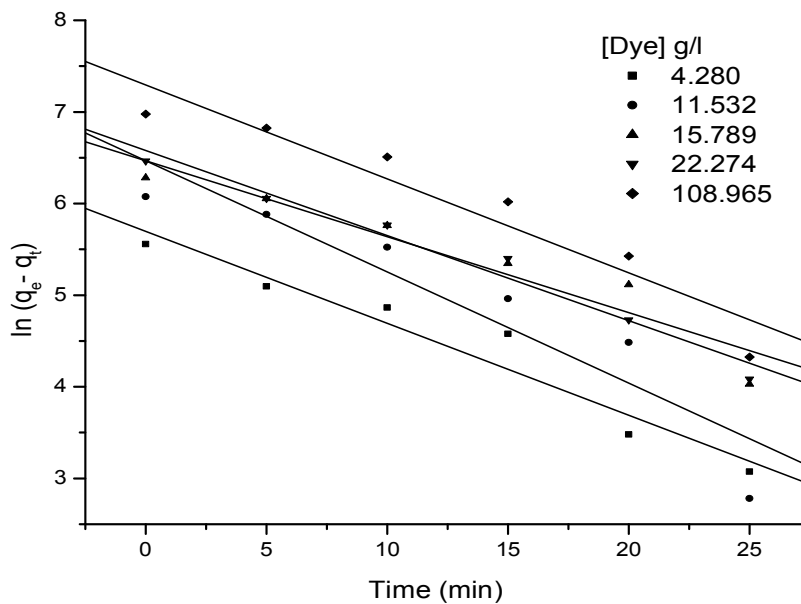


Figure 13. Plot of the pseudo first-order kinetics for the adsorption of DY50 onto TiO_2 -P25 nanoparticles at different dye concentrations.

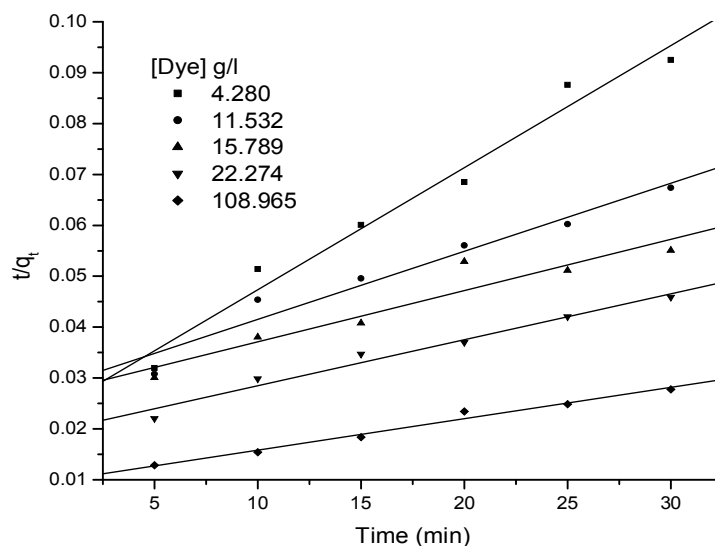


Figure 14: Plot of the pseudo second-order kinetics for the adsorption of DY50 onto TiO₂- P25 nanoparticles at different dye concentrations.

Table 1: Percent degree of degradation (DD %) at λ_{\max} (397nm) for DY50 and the values of $k(\text{min}^{-1})$ for the different loading of TiO₂ in presence of [DY50]= 0.02 mM, time = 65 mins and pH 3.0.

[TiO ₂] g/l	DD%	$k (\text{min}^{-1}) \times 10^3$	$t_{1/2}(\text{min})$	$R_{\text{initial}} (k_{\text{app}} \times C_0) \times 10^6$ (mol l ⁻¹ min ⁻¹)	EE/O(kWh)	r
0.25	80.568	30.44	22.7661	0.608	152.69	0.993
0.5	87.981	31.90	21.72414	0.638	145.70	0.998
1.00	95.034	60.96	11.36811	1.219	76.24	0.999
1.50	92.781	39.31	17.6291	0.786	118.23	0.994

Table 2: Percent degree of degradation (DD %) at λ_{\max} (510nm) for DY50 and the values of $k(\text{min}^{-1})$ for the different dye concentrations in presence of [TiO₂] =1.0 g/l, time = 65 mins and pH 3.0

[Dye] mM	DD%	$k \times 10^3 (\text{min}^{-1})$	$t_{1/2}(\text{min})$	$R_{\text{initial}} (k_{\text{app}} \times C_0) \times 10^6$ (mol l ⁻¹ min ⁻¹)	EE/O (kWh)	r
0.02	95.03	60.96	11.36	1.219	76.24	0.999
0.05	42.08	10.14	68.34	0.202	458.38	0.999
0.07	30.08	5.70	121.579	0.114	815.43	0.995
0.10	13.23	3.51	197.43	0.007	1324.21	0.997
0.50	4.410	0.69	1004.34	0.001	6736.23	0.992

Table 3: Percent degree of degradation (DD %) at λ_{\max} (397nm) for DY50 and the values of $k(\text{min}^{-1})$ for the different pH in presence of [DY50]= 0.02 mM, time = 65 mins.

pH	DD%	$k \times 10^3 (\text{min}^{-1})$	$t_{1/2}(\text{min})$	$R_{\text{initial}} (k_{\text{app}} \times C_0) \times 10^6$ (mol l ⁻¹ min ⁻¹)	EE/O(kWh)	r
1.1	74.698	22.50	30.80	0.450	206.57	0.989
2.2	85.840	39.80	17.41	0.796	116.78	0.999
3.0	95.640	60.96	11.36	1.219	76.24	0.998
4.0	87.341	26.04	26.61	0.520	178.49	0.989
5.2	73.214	24.10	28.75	0.482	192.86	0.985
6.1	66.328	18.50	37.45	0.370	251.24	0.992
7.0	36.239	7.81	88.73	0.156	595.13	0.991
9.3	50.217	11.10	62.43	0.222	418.73	0.998

Table 4: Percent degree of degradation (DD %) at λ_{\max} (510nm) for DY50 and the values of $k(\text{min}^{-1})$ for the different concentrations of H_2O_2 in presence of $[\text{DY50}]=0.02 \text{ mM}$, $[\text{TiO}_2]=1.0 \text{ g/l}$ and $\text{pH } 3.0$.

$[\text{H}_2\text{O}_2]$ mM	DD%	$k (\text{min}^{-1}) \times 10^3$	$t_{1/2}(\text{min})$	$R_{\text{initial}} k_{\text{app}} \times C_0$ ($\text{mol l}^{-1} \text{ min}^{-1}$) $\times 10^6$	EE/O kWh	r
5	83.975	40.67	8.25	1.679	55.34	0.998
10	99.830	90.17	6.94	1.996	46.55	0.999
25	97.831	83.61	7.08	1.956	47.51	0.999
50	96.040	76.87	7.21	1.920	48.39	0.999

Table 5: Langmuir and Freundlich isotherm constants of adsorption of DY50 onto TiO_2 .

Langmuir			Freundlich		
$Q (\text{mg/g TiO}_2)$	$b (\text{ml/mg})$	r	$Q_f (\text{mg/g TiO}_2)$	1/n	r
961.538	0.0268	0.995	111.163	0.372	0.991

Table 6: Pseudo- first and second order kinetic constants for the adsorption of DY50 onto TiO_2 - P25 nanoparticles at different concentrations.

$[\text{DY50}]_0$ (mg/l)	q_e experimental (mg/g)	k_1 (min^{-1})	q_{e1} calculated (mg/g)	r	k_2 (g/mg min) $\times 10^5$	q_{e2} calculated (mg/g)	r
4.280	308.3515	0.070	251.89	0.971	2.466	416.667	0.987
11.532	443.2118	0.075	643.55	0.945	6.376	645.268	0.977
15.789	534.0218	0.082	642.906	0.954	3.776	890.099	0.967
22.274	650.001	0.092	719.099	0.986	4.203	1006.099	0.987
108.965	1021.001	0.102	1470.415	0.957	3.936	1521.71	0.992

4. Conclusion

Fe^{3+} -doped TiO_2 composite nanoparticles with doping amount ($\text{Fe}^{3+} = 0.01\text{wt } \%$) is successfully synthesized using an incipient wet impregnation method. The prepared nanoparticles were characterized by SEM, EDX, XRD and TEM. The results indicate that the size of the TiO_2 nanoparticles decreases on doping amount of Fe^{3+} . The doping of Fe^{3+} can control the conversion of TiO_2 from anatase to rutile and broaden the width of the diffraction peaks of TiO_2 . It is important that an appropriate doping of Fe^{3+} (about 0.01% in our experiment) can markedly improve the catalytic activity of TiO_2 under UV-light irradiation. The degradation of dyes depends on several parameters such as pH, catalyst, substrate and H_2O_2 concentration. The introduction of Fe^{3+} ions in TiO_2 nanoparticles is responsible reducing the photo-generated hole-electron recombination rate. Hence, it is hopeful to use Fe^{3+} -doped TiO_2 as an effective photocatalyst in the degradation of organic contaminants, cleanup of aqueous contaminants especially the aqueous contaminants of dye in the fields of environmental decontamination. Moreover Electrical energy per order (EE/O) was proposed to assess the relative performance of catalytic system used. The adsorption of direct yellow 50, onto TiO_2 Degussa P25 from aqueous solution was also investigated.

References

1. Wongkalasin, P., S. Chavadej, T. (2001) Sreethawong, Photocatalytic degradation of mixed azo dyes in aqueous wastewater using mesoporous-assembled TiO_2 nanocrystal synthesized by a modified sol-gel process, Colloids and Surfaces A: Physicochem. Eng. Aspects 384) 519– 528
2. Konstantinou, I.K., T. A. Albanis, (2004) TiO_2 -assisted photocatalytic degradation of azo dyes in aqueous solution: kinetic and mechanistic investigations: a review, Appl. Catal. B: Environ. 19 1–14
3. Fox, M.A., M.T. Dulay, (1993) Heterogeneous photocatalysis, Chem. Rev. 9) 341–357.
4. [4] Hoffmann, M.R., S.T. Martin, W. Choi, D.W. Bahnemann, Environmental applications of semiconductor photocatalysis, Chem. Rev. 9 (1995) 69–96.
5. Lachheb, H., E. Puzenat, A. Houas, M. Ksibi, E. Elimame, C. Guillard, J. M. Herrmann, Photocatalytic degradation of various types of dyes (Alizarin S, Crocein Orange G, Methyl Red, Congo Red, Methylene Blue) in water by UV-irradiated titania, Appl. Catal. B: Environ. 39 (2002) 75–90.
6. Carp, C. L. Huisman, A. Reller, Photoinduced reactivity of titanium dioxide, Prog. Solid State Chem. 3 (2004) 33–177.
7. Houas, H. Lachheb, M. Ksibi, E. Elaloui, C. Guillard, J. M. Herrmann, photocatalytic degradation pathway of methylene blue in water, Appl. Catal. B Environ. 31 (2001) 145–157.

8. [8]. Vautier, C. Guillard, J. M. Hermann, Photocatalytic degradation of dyes in water: case study of Indigo and of Indigo Carmine, *J. Catal.* 201 (2001) 46–59.
9. So, M.Y. Cheng, J. C. Yu, P. K. Wong, Degradation of azo dye Procion Red MX-5B by photocatalytic oxidation, *Chemosphere* 46 (2002) 905–912.
10. C. Baiocchi, M. C. Brussino, E. Pramauro, A. B. Prevot, L. Palmisano, G. Marci, characterization of methyl orange and its photocatalytic degradation products by HPLC/UV–VIS diode array and atmospheric pressure ionization quadrupole ion trap mass spectrometry, *Int. J. Mass Spectrom.* 21 (2002) 247–256.
11. Y. Ou, J. D. Lin, H. M. Zou, D. W. Liao, Effects of surface modification of TiO₂ with ascorbic acid on photocatalytic decolorisation of an azo dye reactions and mechanisms, *J. Mol. Catal. A: Chem.* 241 (2005) 59–64.
12. N. M. Mahmoodi, M. Arami, N. Y. Limaee, N. S. Tabrizi, Kinetics of heterogeneous photocatalytic degradation of reactive dyes in an immobilized TiO₂ photocatalytic reactor, *J. Colloid Interface Sci.* 295 (2006) 159–164.
13. S. Bitao, W. Ke, B. Jie, M. Hongmei, T. Yongchun, M. Shixiong, S. Shixiong, L. Ziqiang, Photocatalytic degradation of methylene blue on Fe³⁺-doped TiO₂ nanoparticles under visible light irradiation, *Front. Chem. China*, 2 (2007) 364–368.
14. H. M. Sung-Suh, J. R. Choi, H. J. Hah, S. M. Koo, Y. C. Bae, Comparison of Ag deposition effects on the photocatalytic activity of nanoparticulate TiO₂ under visible and UV light irradiation. *J. Photochem. and Photobiol. A: Chem.* 163 (2004): 37–44.
15. Y. Bessekhoud, D. Robert, J. V. Weber, Bi₂S₃/TiO₂ and CdS/TiO₂ heterojunctions as an available configuration for photocatalytic degradation of organic pollutant, *J. Photochem. and Photobiol. A: Chem.* 163 (2004): 569–580
16. Z. Y. Ma, S. X. Min, S. X. She, B. T. Su, Catalytic property of ZnO/conjugated polymer complex particles under natural light. *Chinese J. Appl. Chem.*, 22(2005): 1,137–1,140 (in Chinese)
17. W. Y. Choi, A. Termin, M. R. Hoffmann, The role of metal ion dopants in quantum-sized TiO₂: Correlation between photoreactivity and charge carrier recombination dynamics. *J. Phys. Chem.*, 98 (1994): 13,669–13,679.
18. Y. Yalcin, M. Kilic, Z. Cinar, Fe⁺³-doped TiO₂: A combined experimental and computational approach to the evaluation of visible light activity, *Appl. Catal. B: Environ.*, 99 (2010) 469–477.
19. A. Lopez, A. Bozzi, G. Maseolo, J. Kiwi, *J. photochem. and photobiol. A: Chem.*, 156 (2003) 121-126.
20. Y. Bulut, N. Gozubenli, H. Aydin, Equilibrium and kinetics studies for adsorption of direct blue 71 from aqueous solution by wheat shells. *J. Hazard. Mater.* , 144 (2007) 300-306.
21. A. L. Linsebigler, G. Q. Lu, J. T. Yates, Photocatalysis on TiO₂ surface: Principles mechanisms and selected results. *Chem Rev*, 95(1995): 735–758
22. K. Naeem, F. Ouyang, Preparation of Fe³⁺-doped TiO₂ nanoparticles and its photocatalytic activity under UV light, *Physica B* 405 (2010) 221–226.
23. Kumar, K. Porkodi, F. Rocha, Langmuir–Hinshelwood kinetics – A theoretical study, *Catalysis Comm.*, 9 (2008) 82-84.
24. Behnajady, N. Modirshahla, R. Hamzavi, Kinetic study on photocatalytic degradation of C.I. Acid Yellow 23 by ZnO photocatalyst, *J. Hazard. Mater.* B133 (2006) 226–232.
25. A. A. Khodja, T. Sehili, J. Pilichowski, P. Boule, Photocatalytic degradation of 2 phenyl-phenol on TiO₂ and ZnO in aqueous suspension, *J. Photochem. and Photobiol. A: Chem.* 141 (2001) 231–239.
26. N. Daneshvar, D. Salari, A. R. Khataee, Photocatalytic degradation of azo dye acid red 14 in water on ZnO as an alternative catalyst to TiO₂, *J. Photochem. and Photobiol. A: Chem.* 162 (2004) 317–322.
27. Ahmed, M. G. Rasul, R. Brown, M. A. Hashib, Influence of parameters on the heterogeneous photocatalytic degradation of pesticides and phenolic contaminants in wastewater: A short review, *J. of Environ. Manag.*, 92 (2011) 311-330
28. Mathews, Purification of water with near-UV illuminated suspensions of titanium dioxide. *Water Research*, 24(1990) 653-660.
29. Mathews, Kinetics of photocatalytic oxidation of organic solutes over titanium dioxide catalysis. *J. Catalysis*, 111 (1988) 264-272.
30. Mills, S. Morris, Photo-mineralization of 4-chlororphenol sensitized by titanium dioxide: a study of the initial kinetics of carbon dioxide photogeneration. *J. Photochem. and Photobiology A: Chemistry*, 71 (1993) 75-8.
31. Bahnemann, J. Cunningham, M. A. Fox, E. Pelizzetti, P. Pichat, N. Serpone, in: R.G. Zepp, G.R. Heltz, D.G. Crosby (Eds.), *Aquatic Surface Photochemistry*, Lewis Publishers, Boca Raton, 1994, p. 261.
32. S. Tunesi, M. Anderson, Influence of chemisorption on the photodecomposition of salicylic acid and related compounds using suspended titania ceramic membranes, *J. Phys. Chem.* 95 (1991) 3399–3405.
33. M.S.T. Concalves, A.M.F. Oliveira-Campos, M.M.S. Pinto, P.M.S. Plasencia, M.J.R.P. Queiroz, Photochemical treatment of solutions of azo dyes containing TiO₂, *Chemosphere*, 39 (1991) 781-792.
34. C. Guillard, J. Disdier, C. Monnet, J. Dussaud, S. Malato, J. Blanco, M.I. Maldonado, J.M.

- Herrmann, Solar efficiency of a new deposited titania photocatalyst: chlorophenol, pesticide and dye removal applications, *Appl. Catal. B: Environ.*, 46 (2003) 319–332.
35. L.B. Reutergerath, M. Iangpashuk, Photocatalytic decolorization of reactive azo dye: a comparison between TiO₂ and CdS photocatalysts, *Chemosphere* 35 (1997) 585–596.
 36. W.Z. Tang, H. An, UV/TiO₂ photocatalytic oxidation of commercial dyes in aqueous solutions, *Chemosphere*, 31 (1995) 4158–4170.
 37. W. Baran, A. Makowski, W. Wardas, The effect of UV radiation absorption of cationic and anionic dye solutions on their photocatalytic degradation in the presence of TiO₂, *Dyes and Pigm.* 76 (2008) 226–230.
 38. W. Baran, A. Makowski, W. Wardas, The influence of FeCl₃ on the photocatalytic degradation of dissolved azo dyes in aqueous TiO₂ suspensions, *Chemosphere*, 53 (2003) 87–95.
 39. W.Z. Tang, H. An, Photocatalytic degradation kinetics and mechanism of acid blue 40 by TiO₂/UV in aqueous solution, *Chemosphere*, 31 (1995) 4171–4183.
 40. K. H.Wang, Y. H. Hsieh, C. H.Wu, C. Y. Chang, The pH and anion effects on the heterogeneous photocatalytic degradation of o-methylbenzoic acid in TiO₂ aqueous suspension, *Chemosphere*, 40 (2000) 389–394.
 41. M. Styliidi, D.I. Kondarides, X.E. Verykios, Pathways of solar light-induced photocatalytic degradation of azo dyes in aqueous TiO₂ suspension, *Appl. Catal. B: Environ.*, 40 (2003) 271–286.
 42. T. Zhang, T. Oyama, S. Horikoshi, H. Hidaka, J. Zhao, N. Serpone, Photocatalyzed N-demethylation and degradation of methylene blue in titania dispersions exposed to concentrated sunlight, *Sol. Energy Mater. Sol. Cells* 73 (2002) 287–303.
 43. N. Daneshvar, D. Salari, A. R. Khataee, Photocatalytic degradation of azo dye acid red 14 in water: Investigation of the effect of operational parameters. *J. Photochem. and Photobiol. A: Chemistry*, 157 (2003), 111–116.
 44. S. R. Cater, M. I. Stefan, J. R. Bolton, A. Safarzadeh-Amiri, UV/H₂O₂ treatment of methyl tert-butyl ether in contaminated waters. *Environ. Sci. Technol.*, 34 (2000) 659–662.
 45. Y. J. Lin, A.Lee, L.S. Teng, and H.T. Lin, Effect of experimental factors on nitrobenzaldehyde photoisomerization, *Chemosphere*, 48 (2002) 1–8.
 46. M.I. Stefan, J. R.Bolton, Fundamental approach to the fluence-based kinetic and electrical energy efficiency parameters in photochemical degradation reactions: polychromatic light, *J Environ Eng Sci/Rev Gen Sci Env*, 4 (2005) S13–S18.
 47. P. F. Yan, J. Q. Wang, X. Jiang, D. R. Zhou, H. G. Fu, Preparation and photocatalytic properties of iron-doped TiO₂ nanocrystal. *Mater. Sci. Technol.* 10 (2002) 28–31 (in Chinese)
 48. V. Gokmen, A. Serpen, Equilibrium and kinetic studies on the adsorption of dark colored compounds from apple juice using adsorbent resin. *J. Food Eng.* 53 (2002) 221–227.
 49. C. H. Chiou, C. Y. Wu, R. S. Juang, Influence of operating parameters on photocatalytic degradation of phenol in UV/TiO₂ process. *Chem. Engin. J.* 139 (2008) 322–329.
 50. N. K. Lazaridis, D. D. Asouhidou, Kinetics of sorptive removal of chromium (VI) from aqueous solutions by calcined Mg–Al–CO₃ hydrotalcite, *Water Res.* 37 (2003) 2875–2882.
 51. M. d. T. Uddin, M. D. A. Islam, S. Mahmud, M. d. Rukanuzzaman, Adsorptive removal of methylene blue by tea waste, *J. Hazard. Mater.* 164 (2009) 53–60
 52. I. Langmuir, Adsorption of gases on plain surfaces of glass mica platinum. *J. Am. Chem. Soc.* 1918; 40: 1361–1403.
 53. H. Freundlich, Adsorption in solution, *Z. Phys. Chemie*, 57 (1906) 384–470.
 54. A. S. Ozcan, B. Erdem, A. Ozcan, Adsorption of Acid Blue 193 from aqueous solutions onto Na-bentonite and DTMA-bentonite. *J. Colloid Interf. Sci.*, 280 (2004) 44–54.
 55. S. Lagergren, Zur theorie der sogenannten adsorption geloster stoffe, *K. Sven. Vetenskapsakad. Handl.*, 24 (1898) 1–39.
 56. P.K. Malik, Dye removal from wastewater using activated carbon developed from sawdust: adsorption equilibrium and kinetics. *J. Hazard. Mater. B* 113 (2004) 81–88.
 57. Y.S. Ho, G. McKay, The kinetics of sorption of divalent metal ions onto sphagnum moss peat, *Water Res.* 34 (2000) 735–742.
 58. Y. S. Ho, Comments on “an adsorption and kinetic study of lac dyeing on silk”. *Dyes and Pigments*, 72 (2007) 134–6.